Int. J. Heat Mass Transfer. Vol. 36, No. 12, pp. 3029–3042, 1993
Printed in Great Britain

0017–9310/93 $6.00 + 0.00

Mixed convective flow with mass transfer in a horizontal rectangular duct heated from below simulated by the conditional Fourier spectral analysis

IWAO HOSOKAWA and YOSHINORI TANAKA
Department of Mechanical and Control Engineering, University of Electro-Communications, Chofu, Tokyo 182, Japan

and

KIYOSHI YAMAMOTO
National Aerospace Laboratory, Chofu, Tokyo 182, Japan

(*Received* 30 *October* 1992 *and in final form* 17 *December* 1992)

Abstract—With application to a horizontal chemical vapor deposition apparatus in mind, mixed convection and mass transfer in a horizontal rectangular duct heated from below are numerically investigated. The computer simulation is carried out based on the conditional Fourier spectral method recently developed by the authors. Unsteady flow states occurring at rather high Grashof numbers are highlighted as good conditions for providing the spanwise uniformities of time-averaged temperature distribution and time-averaged Sherwood number distribution on the substrate at the duct bottom.

1. INTRODUCTION

FORCED flows in a horizontal rectangular duct with the top wall cold, the bottom wall hot, and the side walls insulated or with a proper temperture have recently caught strong engineering attention in relation to the chemical vapor deposition (CVD) apparatus which is important in semiconductor manufacturing and others. Practically, chemical matters included in carrier gas flowing in a duct are expected to react on a substrate set at the hot bottom and be deposited there to make a uniform thin layer.

Although a few works [1–3] had preceded, a typical numerical calculation of the flows in such a duct was performed by Moffat and Jensen [4, 5], who solved the steady set of the compressible Navier–Stokes equation, energy equation, and concentration equations for dilute reactants with proper chemical kinetics with special simplifying assumptions of pressure decomposition and no longitudinal diffusion of momentum, temperature and concentration. They showed the appearance of a symmetric pair of buoyancy-driven longitudinal rolls for Rayleigh numbers (Ra) typical in a CVD reactor, and that the sense of the rolls depends on the side wall temperature condition such as adiabatic or isothermal. Without the special assumptions described above, Nyce *et al.* [6] solved numerically the steady Boussinesq set of equations and identified the growth of a pair of steady rolls in the duct with aspect ratio 2, but associated with a flow asymmetry with respect to the mid-width plane or even unsteadiness for a smaller Reynolds number (Re) at a fixed Ra. They concluded that the mixed flow must not be parabolic, as Moffat and Jensen assumed, but elliptic. On the other hand, Evans and Greif [7] solved numerically the time-dependent set of the compressible Navier–Stokes equation and energy equation to find the occurrence of travelling waves in the mixed flow for a larger Grashof number (Gr), i.e. a smaller Re^2/Gr, and predicted a positive effect of the interaction of transverse, travelling waves and longitudinal rolls on CVD, even though how positive it would be remained still a question.

It is important in this situation to recall the experiments of Mori and Koizumi [8], Koizumi and Hosokawa [9], and Mori *et al.* [10], which showed that the longitudinal rolls at a fully developed flow state in a duct could be controlled by the side wall temperature profile and even destroyed into an unsteady chaotic state so that the time-averaged temperature in the duct became spanwise uniform. It is now known [11] that the naphthalene evaporation as a reverse phenomenon of CVD can occur very uniformly over time in this chaotic state of the mixed flow, while it cannot in the steady state with the rolls; there was no clear difference detected in the roughness (or ruggedness) of the naphthalene surface after evaporation between the steady and the unsteady flow case, so that any striation on the CVD surface which may be apprehended would not occur due to the flow unsteadiness of this degree. A main motivation of the present

NOMENCLATURE

C concentration field of a dilute reactant normalized by its saturation concentration at the bottom temperture
C_0 basic dimensionless concentration field
c $C-C_0$
De equivalent hydraulic diameter [m]
$\mathbf{e}_x, \mathbf{e}_z$ unit vectors in the x and z directions, respectively
$\mathbf{e}_1, \mathbf{e}_2$ unit vectors orthogonal to $\mathbf{k}$ in wavenumber space
g acceleration of gravity [m s^{-2}]
Gr Grashof number (based on De)
$\mathbf{k}$ wavenumber vector
k, k_x, k_y, k_z magnitude and x-, y-, and z-components of $\mathbf{k}$
L_x, L_y, L_z longitudinal, spanwise, and vertical side-lengths of the computational space
l $(k_y^2+k_z^2)^{1/2}$
Nu Nusselt number
n_x, n_y, n_z integers
P dimensionless pressure field
P_0 basic dimensionless pressure field
p $P-P_0$
Pr Prandtl number
Ra Rayleigh number
Re Reynolds number
Sc Schmidt number
Sh Sherwood number
T absolute temperature field [K]
T_t, T_b values of T at the top and the bottom wall, respectively [K]
t time variable normalized by De/U_A
$\mathbf{U}$ velocity field normalized by U_A
U_A average speed of the forced flow [m s^{-1}]
U_0 basic dimensionless velocity field
$\mathbf{u}$ $\mathbf{U}-U_0\mathbf{e}_x$
u_z z-component of $\mathbf{u}$
u_1, u_2 solenoidal components of $\mathbf{u}$
$\mathbf{x}$ (x, y, z)
x, y, z longitudinal, spanwise, and vertical coordinates normalized by De.

Greek symbols

β thermal expansion coefficient of gas [K^{-1}]
Θ dimensionless temperature field, $(T-T_t)/(T_b-T_t)-1/2$
Θ_0 basic dimensionless temperature field
Θ_w profile of Θ at the side walls
θ $\Theta-\Theta_0$
κ thermal diffusivity of gas [m^2 s^{-1}]
ν kinematic viscosity of gas [m^2 s^{-1}]
ρ_0 density of the gas at the reference level, $z=0$ [kg m^{-3}].

research is to identify this interesting phenomenon of heat and mass transfer in a numerical way.

If chaos or turbulence is included, the method of solution of the time-dependent set of basic equations should be accurate enough. On this point, a spectral method is superior to any finite-difference method. However, the well known Chebyshev spectral method is unpioneered as yet, so much as to be applied to such a three-dimensional (3D) duct problem as treated here. Therefore, we adopt the conditional Fourier spectral method recently developed by the authors [12–14] to solve the basic equations mainly with $32\times64\times32$ modes. This resolution is barely fine enough to treat a strong turbulence but able to investigate a pre-turbulent chaos in which very high wavenumber modes are not excited. (If a finer resolution like 128^3 is available, a strongly turbulent flow can be extensively treated [13].) The Boussinesq set of equations is used here as a first tool. Of course, it may be imperfect for describing reality, but we can get a characteristic feature of the unstable mixed flows even if not offering a perfect accord of numerical results with experiment. In this work, we take the aspect ratio of the infinitely long horizontal duct as 2, $Re = 220$, Prandtl number $(Pr) = 0.71$, and Schmidt number $(Sc) = 2.5$, which is close to the CVD condition of GaAs in accordance with the above-described experiment [8–10], and change Gr up to 4.8×10^6. Mainly, the side walls are assumed as perfectly conducting, so that the temperature there changes linearly from top to bottom. The condition close to this was covered by the experiment. The supercomputers used are FACOM VP-400 and -2600 at the National Aerospace Laboratory (Japan).

2. FORMULATION

2.1. *The Boussinesq set of equations*

As shown in Fig. 1, we take $x\in[0, L_x]$ in the horizontal forced-flow direction, $y\in[-L_y, L_y]$ spanwise, and $z\in[-L_z, L_z]$ in the vertical direction. The Bous-

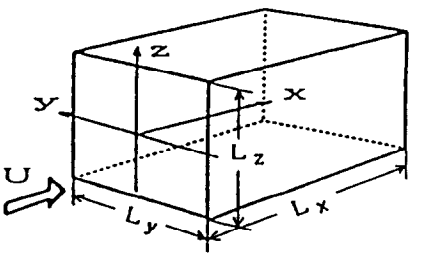

FIG. 1. Configuration of the horizontal rectangular duct.

sinesq set of equations for the dimensionless velocity vector $\mathbf{U}$ and temperature Θ in our system is

$$\mathrm{D}\mathbf{U}/\mathrm{D}t = -\nabla P + (1/Re)\Delta\mathbf{U} + (Gr/Re^2)\Theta\mathbf{e}_z \quad (1)$$

$$\mathrm{div}\,\mathbf{U} = 0 \quad (2)$$

$$\mathrm{D}\Theta/\mathrm{D}t = 1/(Pr\,Re)\Delta\Theta. \quad (3)$$

Here, $\mathrm{D}/\mathrm{D}t$ denotes the substantive time-derivative; length is normalized by the equivalent hydraulic diameter of the duct De, and velocity by the average speed of the forced flow U_A. The parameters are defined as $Re = U_A De/\nu$, $Gr = g\beta(T_b - T_t)De^3/\nu^2$ and $Pr = \nu/\kappa$. Θ is related to the real absolute temperature T as

$$\Theta = (T - T_t)/(T_b - T_t) - 1/2 \quad (4)$$

so that the reference point of gas density ρ_0 is taken in the middle plane of the duct ($z = 0$).

The boundary conditions for $\mathbf{U}$ and Θ are

$$\mathbf{U}(x, \pm L_y/2, z) = \mathbf{U}(x, y, \pm L_z/2) = 0 \quad (5)$$

$$\Theta(x, \pm L_y/2, z) = \Theta_w(z), \quad \Theta(x, y, L_z/2) = -1/2,$$
$$\Theta(x, y, -L_z/2) = 1/2 \quad (6)$$

where Θ_w is the prescribed profile of the side wall temperature. Both the velocity and temperature fields are assumed to be periodic in x with period L_x, as usually done in spectral methods. We introduce the steady basic fields $U_0(y, z)$ and $\Theta_0(y, z)$ that satisfy

$$0 = -\mathrm{d}P_0/\mathrm{d}x + (1/Re)(\partial^2/\partial y^2 + \partial^2/\partial z^2)U_0 \quad (7)$$

$$0 = (\partial^2/\partial y^2 + \partial^2/\partial z^2)\Theta_0 \quad (8)$$

subject to equations (5) and (6), respectively, and consider the new fields: $\mathbf{u} = \mathbf{U} - U_0\mathbf{e}_x$, $p = P - P_0$, and $\theta = \Theta - \Theta_0$. U_0 is known together with P_0 [15], and Θ_0 is easy to solve for. Thus, we have

$$\partial\mathbf{u}/\partial t = -\nabla p + (1/Re)\Delta\mathbf{u} - U_0\,\partial\mathbf{u}/\partial x - \mathbf{u}\cdot\nabla(U_0\mathbf{e}_x + \mathbf{u}) + (Gr/Re^2)(\Theta_0 + \theta)\mathbf{e}_z \quad (9)$$

$$\mathrm{div}\,\mathbf{u} = 0 \quad (10)$$

$$\partial\theta/\partial t = 1/(Pr\,Re)\Delta\theta - U_0\,\partial\theta/\partial x - \mathbf{u}\cdot\nabla(\Theta_0 + \theta). \quad (11)$$

Since U_0 and Θ_0 satisfy equations (5) and (6), the boundary conditions for u and θ are simply that both of them vanish on all the walls of the duct.

2.2. *Concentration equation*

When a dilute reactant in the gas exists for CVD, we have a single concentration equation for the reactant in the same form as equation (3) with Schmidt number (Sc) in place of Pr, assuming that it is a passive scalar. We treat the dimensionless concentration C normalized by the saturation value at the bottom temperature. In this case, the boundary condition is

$$\partial C/\partial y\,(x, \pm L_y/2, z) = \partial C/\partial z\,(x, y, L_z/2) = 0,$$
$$C(x, y, -L_z/2) = 0 \quad (12)$$

on the basis of fast reaction on the substrate. In order to guarantee the steady existence of the reactant in the flow, a nontrivial basic field C_0 is introduced, which satisfies

$$0 = (\partial^2/\partial x^2 + \partial^2/\partial z^2)C_0. \quad (13)$$

Then, the equation for $c = C - C_0$ is similar to equation (11), but with the boundary condition (12) and the periodicity in $[0, L_x]$. The solution of (13) with (12) is taken here as

$$C_0(x, z) = (4/\pi)\Sigma_{m=0}[1/(2m+1)] \times \sin[(2m+1)\pi(z + L_z/2)/(2L_z)] \times \exp[-(2m+1)\pi x/(2L_z)] \quad (14)$$

which means that the basic density distribution of the reactant is uniform as 1 at the cross-section $x = 0$ and exponentially decays downstream.

Finally, it may be noted that the present formulation can be used for the concentration of an evaporated matter from the bottom surface by reading C and C_0 as $1 - C$ and $1 - C_0$, respectively.

3. METHOD OF SOLUTION

3.1. *Fourier transformation*

The Fourier spectral method is most convenient for the case when the space in question is rectangular, though it needs a special care of the boundary condition of treated fields. Let us consider the transformation

$$\mathbf{u}(\mathbf{x}, t) = \Sigma u(\mathbf{k}, t)\exp(i\mathbf{k}\cdot\mathbf{x}) \quad (15)$$

$$\theta(\mathbf{x}, t) = \Sigma\theta(\mathbf{k}, t)\exp(i\mathbf{k}\cdot\mathbf{x}) \quad (16)$$

where $\mathbf{k} = (2\pi n_x/L_x, 2\pi n_y/L_y, 2\pi n_z/L_z)$, and n_x, n_y, and n_z are integers. Hence we can easily obtain the Fourier transform of equations (9), (10), and (11). The nonlinear convolution terms in it can be calculated as the Fourier transforms of products of the relevant fields in the physical space, in which process the fast Fourier transformation (FFT) technique is indispensably used.

On the other hand, the boundary conditions place the following restrictions to $\mathbf{u}$ and θ:

$$\Sigma_{n_x}(-1)^{n_x}\mathbf{u}(\mathbf{k}, t) = 0, \quad \Sigma_{n_z}(-1)^{n_z}\mathbf{u}(\mathbf{k}, t) = 0 \quad (17)$$

$$\Sigma_{n_x}(-1)^{n_x}\theta(\mathbf{k}, t) = 0, \quad \Sigma_{n_z}(-1)^{n_z}\theta(\mathbf{k}, t) = 0. \quad (18)$$

These limit the space spanned by $u(\mathbf{k}, t)$ and $\theta(\mathbf{k}, t)$ into the special hyperplanes defined by equations (17) and (18). Therefore, to solve the problem we have only to re-express $u(\mathbf{k}, t)$ and $\theta(\mathbf{k}, t)$ in terms of the complete orthogonal hypervectors in the hyperplanes, which are found by a multi-dimensional orthogonal transformation, and then to follow the new dynamics for these hypervectors [13]. Such manipulations can be easily carried out by a supercomputer.

3.2. *Solenoidal field representation*

A solenoidal field automatically satisfying equation (10) is simply constructed in the Fourier space as

$$\mathbf{u}(\mathbf{k},t) = u_1(\mathbf{k},t)\mathbf{e}_1(\mathbf{k}) + u_2(\mathbf{k},t)\mathbf{e}_2(\mathbf{k}) \quad (19)$$

$$\mathbf{e}_1(\mathbf{k}) = (-l/k, k_x k_y/(kl), k_x k_z/(kl)) \quad (20)$$

$$\mathbf{e}_2(\mathbf{k}) = (0, -k_z/l, k_y/l) \quad (21)$$

where $l = (k_y^2 + k_z^2)^{1/2}$ and $k = (k_x^2 + k_y^2 + k_z^2)^{1/2}$. Another great advantage of this representation of $\mathbf{u}$ is that the contribution of the pressure term disappears entirely from the momentum equation (9), since $\mathbf{u}$ in equation (19) has no component proportional to $\mathbf{k}$. Therefore, the dynamics for (u_1, u_2) is much simpler than expected. To avoid the aliasing error in the collocation process, the so-called 2/3 rule is applied [16]. As a result, time integration becomes very easy and a high-order Runge–Kutta method can be used. Here, the fourth-order scheme is used. (The fineness of time step interval is varied for each case so as to insure a sufficient accuracy.) It is very significant that we guarantee exactly the zero-divergence of $\mathbf{u}$ and have no load to calculate the pressure p at each time step, because we have relatively rare chances to be contaminated by round-off errors. The absolute superiority in smallness of round-off errors of using spectral methods and FFT over all the others to solve a partial differential equation was well argued by Canuto *et al.* [16]; even in the case with the pressure term involved as in the other spectral methods, e.g. using the Chebyshev polynomial series, round-off errors influence only several digits of solutions and then the calculation of double-precision is generally acceptable.

3.3. *Treatment of concentration field*

The concentration field c can be Fourier-transformed similarly to equation (16) but only with $k_z = \pi n_z/L_z$, so that c is no longer periodic in $[-L_z/2, L_z/2]$. The boundary condition (12) leads to

$$\Sigma_{n_y}(-1)^{n_y} k_y c(\mathbf{k},t) = 0, \quad \Sigma_{n_z} \exp(i\pi n_z/2) k_z c(\mathbf{k},t) = 0,$$
$$\Sigma_{n_z} \exp(-i\pi n_z/2) c(\mathbf{k},t) = 0. \quad (22)$$

3.4. *Other factors*

3.4.1. *Initial condition.* In order to reach a fully developed state in the present problem, it is necessary and sufficient to give a non-zero initial value to not all but some of $\mathbf{u}(\mathbf{k},0)$, even if θ or c starts from zero. Here, normal–random initial disturbances of the order of 10^{-6} are used for the lowest $9 \times 19 \times 9$ wavenumber modes of $\mathbf{u}(\mathbf{k},0)$ except for $\mathbf{u}(0,0) = 0$. (The order of magnitude of this disturbance is larger than expected round-off errors.) There is the possibility to have a different final state for a different initial condition if there are a plural number of attractors in the phase space, particularly in a chaotic flow case, but it is out of scope here to investigate the number of attractors.

3.4.2. *Geometry of the duct.* The aspect ratio is chosen as 2, and basically $L_x = 3\pi$, $L_y = 1.5$ and $L_z = 0.75$ are taken in units of De.

4. RESULTS

4.1. *Steady states*

4.1.1. *Case of cooled side walls.* When the side walls are cooled just as in the work of Moffat and Jensen [5], the flow becomes quite steady and two-dimensional. In this case, we have $\Theta_w(z) = -1/2$. The result for $Re = 220$ and $Gr = 480\,000$, which is typical as a CVD condition [8–10], is seen in Fig. 2. The time-evolution of the Fourier wave modes indicated by $|\mathbf{u}(k_x, k_y, k_z)|^2$ is seen in Fig. 2(a). In the figure, the 24 (note $\mathbf{u}(0,0) = 0$) modes with $n_x = 0$ are indicated by (originally various colours for various n_y) lines with various marks (for various n_z) as illustrated in the right lattice, while all those with $n_x = 1$ and 2 are indicated, respectively, by 25 black and 25 grey lines with no marks. (These indications will be the same for Figs. 4(a), 5(a)–(c), 6(a) and 8(a).) All three-dimensional (3D) modes of $\mathbf{u}$ disappear and only 2D modes with $|\mathbf{u}(0, k_y, k_z)|^2$ survive as seen in the figure, so that the symmetric two longitudinal rolls are formed steadily as in Fig. 2(b) with a down-flow along the wall, and the temperature contour of $\Theta + 1/2$ in a cross-section is not horizontally uniform as in Fig. 2(c). The experimental values by Mori and Koizumi [8] observed at the locations indicated by circles are inserted in the figure. This type of flow is quite insensitive to initial conditions, and maintained up to a much higher value of Gr. Of course, the flow is stable for any disturbance either bigger or smaller than round-off errors.

In Fig. 3(a) is shown the Sherwood number (Sh) contour on the bottom wall for this case. There is a deep valley seen along the center-line in the substrate. The spanwise non-uniformity of deposition is obvious. We note that $L_x = 3\pi$ in this figure and the longitudinal length is very much abridged. Sh ranges from 5.0 to 21.75.

4.1.2. *Case of perfectly conducting side walls.* For $Re = 220$ and the wall temperature $\Theta_w(z) = -z$, we have a steady flow in the duct when Gr is small. Both $\mathbf{u}$ and θ extinguish for Gr less than 7837, that corresponds to the critical Rayleigh number (Ra) for aspect ratio 2 by Lee *et al.* [17]. Beyond this critical value until $Gr \sim 10^5$, $\mathbf{u}$ and θ evolve to reach a certain steady state, as is seen in Fig. 4(a) for $Gr = 24\,000$, at which the steady secondary flow makes a symmetric pair of longitudinal convection rolls, as seen in Fig. 4(b), and all the longitudinal modes of $\mathbf{u}$ with $k_x \neq 0$ are not excited at all but decay, so that the flow remains completely two-dimensional after an initial transient time. With increasing Gr, however, the constitution of modes changes, the energy of $\mathbf{u}$ increases markedly, and the temperature contour in Fig. 4(c) evolves from mild to boundary-layer type with steep gradients near the top and bottom walls. These steady flows are considered to be approachable by all steady two-dimensional methods using the Boussinesq set (including finite-difference method with much larger round-off errors).

Here, we note an interesting fact that another pair

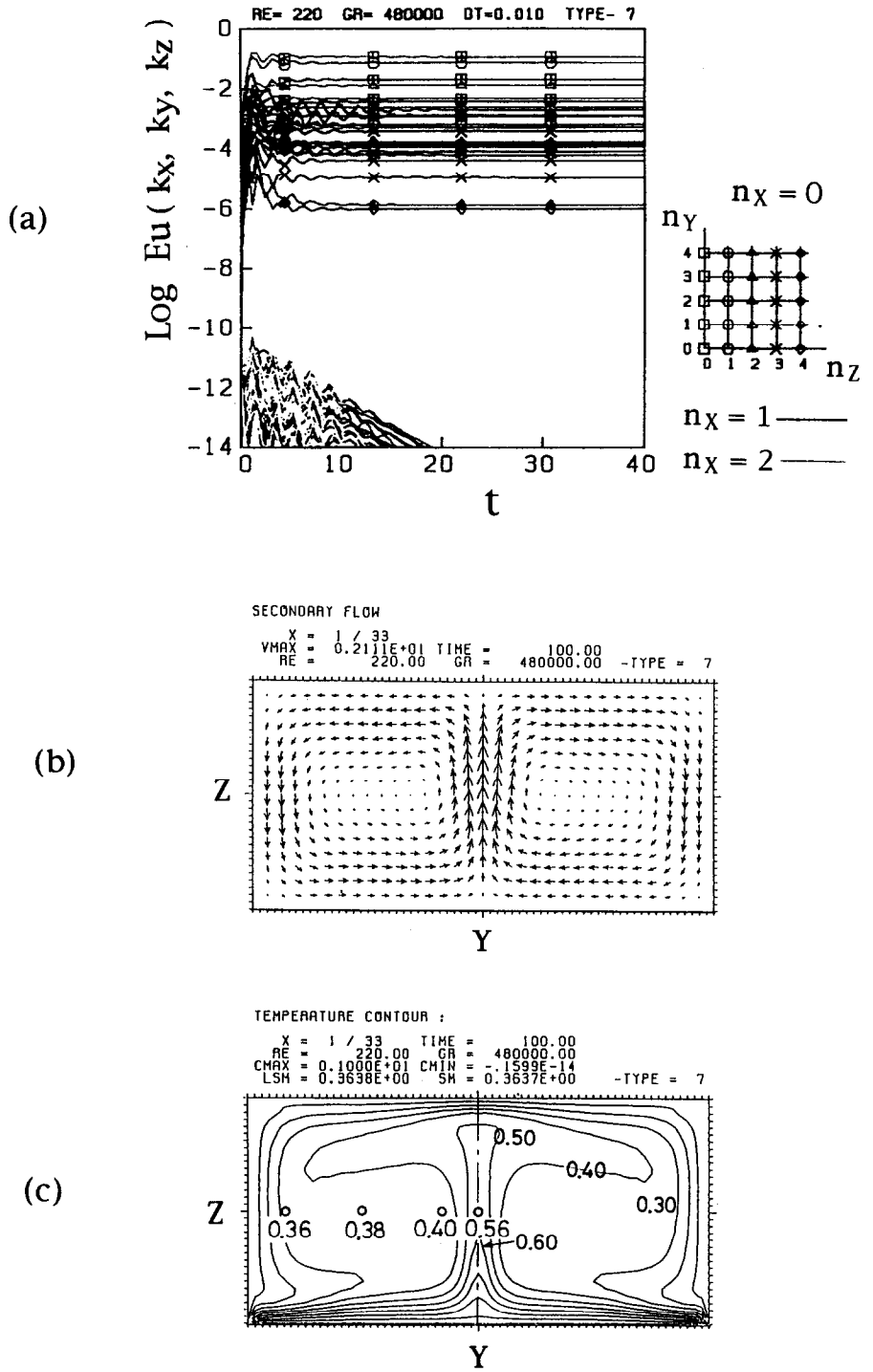

FIG. 2. (a) Evolution of $|\mathbf{u}(k_x, k_y, k_z)|^2$ for the case of $\Theta_w(z) = -1/2$, $Re = 220$, $Gr = 480\,000$ and $L_x = 3\pi$. (b) The secondary flow in the cross-section for the same case. The magnitude of an arrow is normalized by the maximum secondary flow speed. (c) Temperature contour in the cross-section for the same case. Experimental values by Mori and Koizumi [8] at various positions are added for comparison.

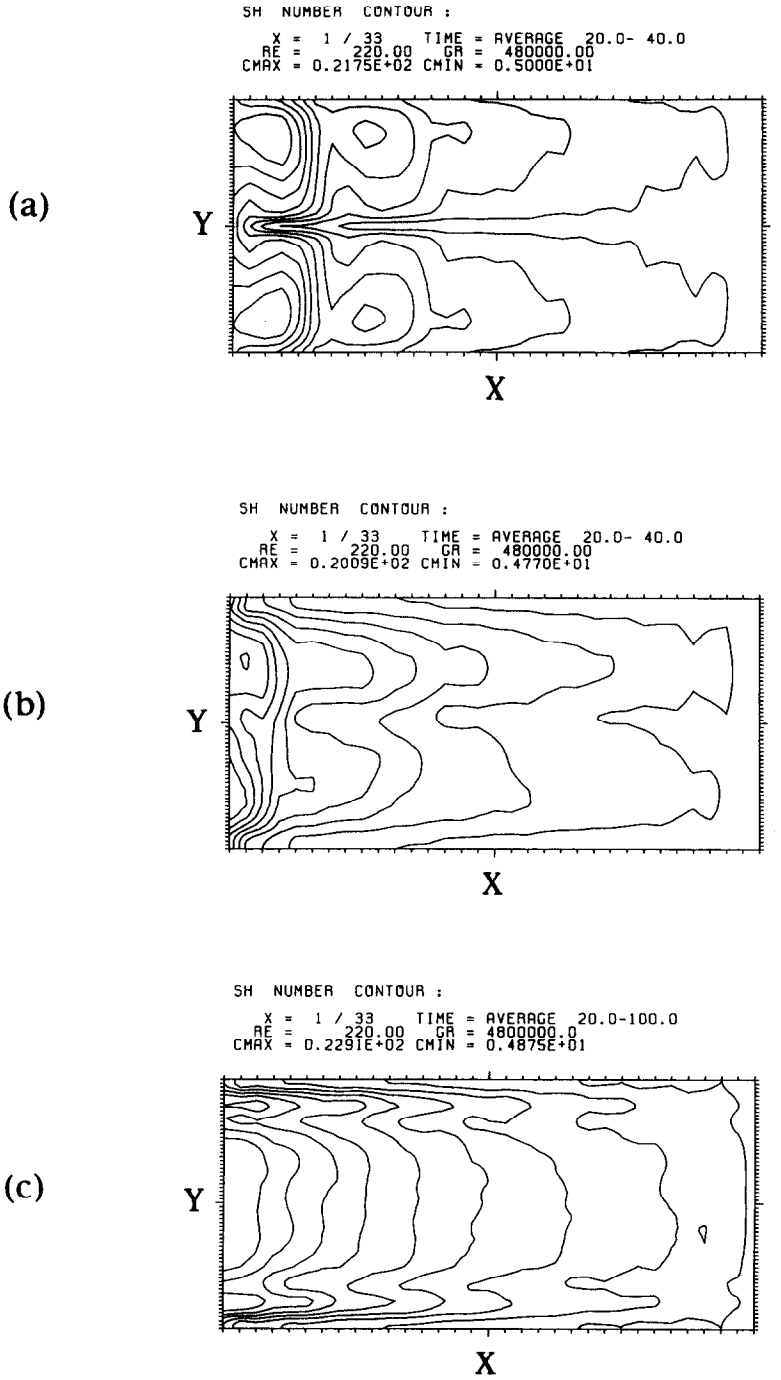

FIG. 3. (a) Sherwood number contour on the bottom for the cooled wall case shown in Fig. 2. (b) Time-averaged Sherwood number contour on the bottom wall for the case in Fig. 6 except with $L_y = 3\pi$. (c) That for the case in Fig. 8.

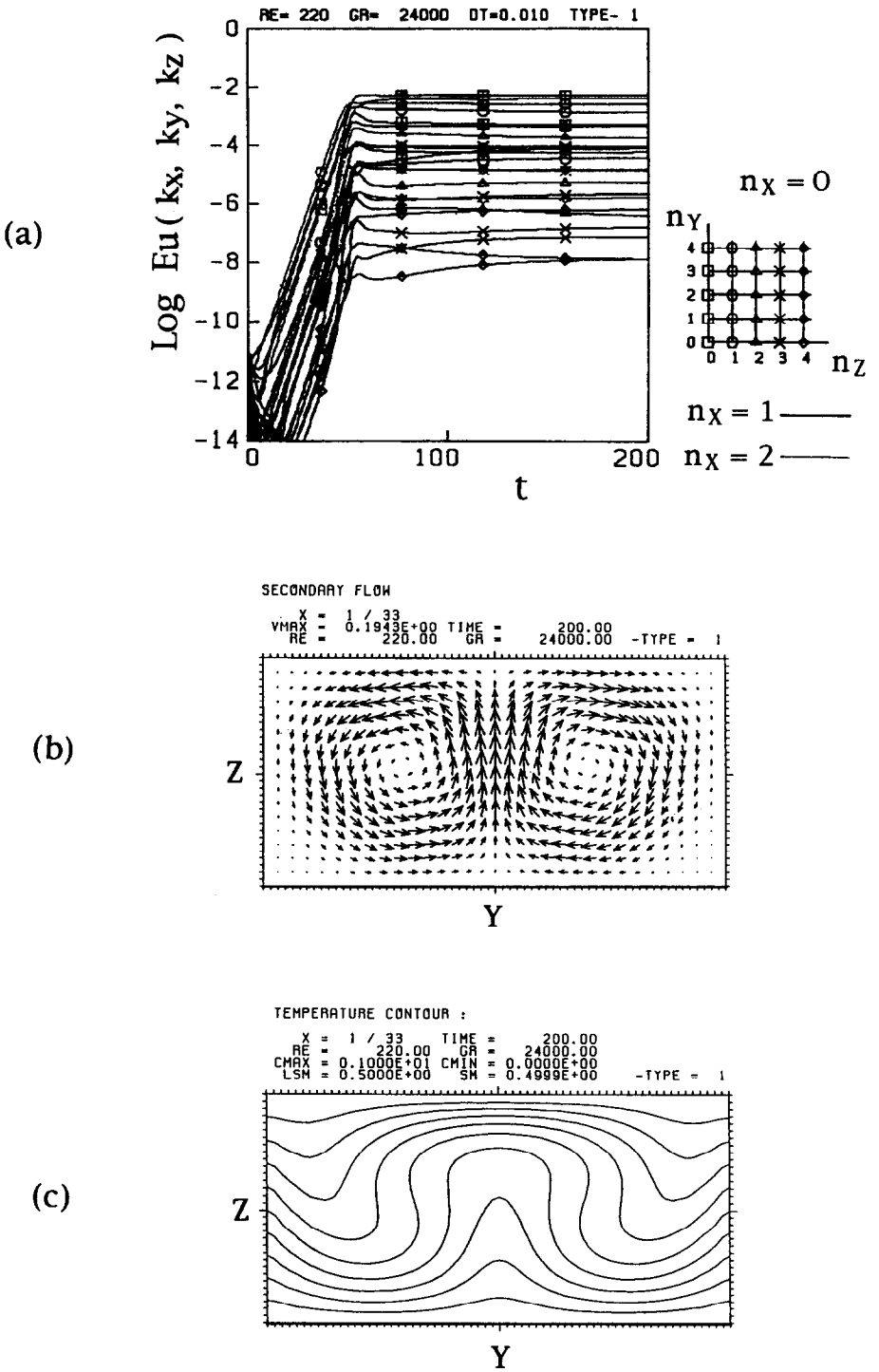

FIG. 4. (a) Evolution of $|\mathbf{u}(k_x, k_y, k_z)|^2$ for the case of $\Theta_w(z) = -z$, $Re = 220$, $Gr = 24\,000$ and $L_x = 3\pi$. (b), (c) The same as in Fig. 2 on this condition, after the steady state has been achieved.

of rolls having the reverse senses can also appear for the present (antisymmetric) profile of $\Theta_w(z) = -z$. This can be understood from the antisymmetry of equations (9)–(11) with respect to z: $u_z(z) = -u_z(-z)$ and $\Theta(z) = -\Theta(-z)$. This has actually been verified by reversing the initial value of $\mathbf{u}$. Thence, this kind of duality of solution can be avoided only by taking a Θ_w without antisymmetry. In fact, when the side walls are hot or cold as compared with the inside average, the sense of rolls is determined so as to be consistent with natural convection to occur on the walls [18, 19].

4.2. *Unsteady states*

Here, only the case of perfectly conducting walls is treated. The case of cooled walls is much stabler; to make it unsteady, an extremely high Gr would be necessary.

4.2.1. *2D unsteady states.* If the initial disturbance field of $\mathbf{u}$ is limited to be two-dimensional ($k_x = 0$), the same steady state as described in the preceding section is stable up to $Gr = 4.2 \times 10^6$ for $Re = 220$, and becomes unstable at $Gr = 4.25 \times 10^6$ to oscillate periodically as is seen in Fig. 5(b). For $Re = 90$, it is unstable already at $Gr = 4.2 \times 10^6$ as in Fig. 5(c), and

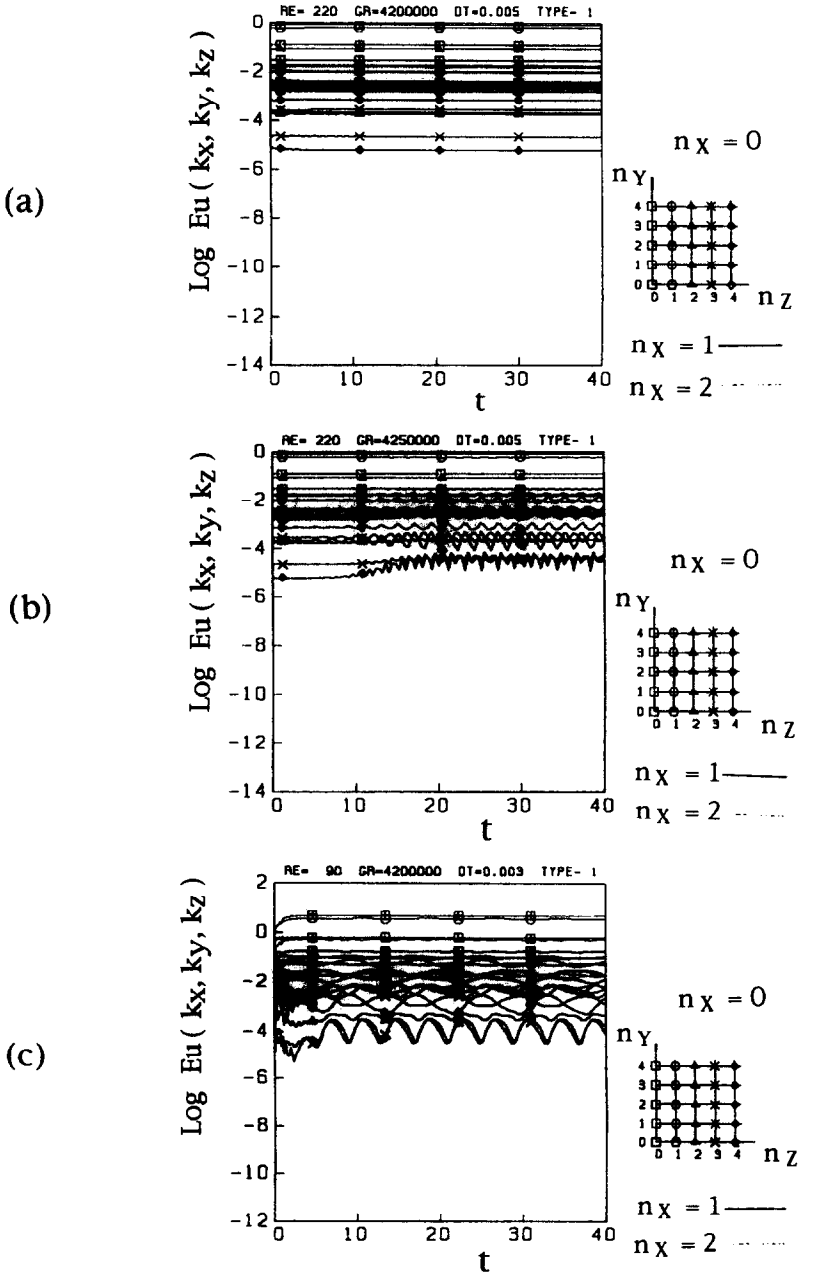

FIG. 5. (a) Evolution of $|\mathbf{u}(k_x, k_y, k_z)|^2$ for the case of $\Theta_w(z) = -z$, $Re = 220$, $Gr = 4.2 \times 10^6$ and $L_x = 3\pi$, when the initial disturbance field is limited to two-dimensional. (b) The same as (a) but for $Gr = 4.25 \times 10^6$. (c) The same as (a) but for $Re = 90$.

then a smaller value of Re^2/Gr is enough to cause an unsteady state. It may be noted that well-defined travelling waves occur in the 2D direction in these cases.

Here, the importance and utility of these evolutional Fourier spectrographs (EFS) should be stressed in studying unsteady states of the system. It includes all the information of the system trajectory, which may approach any kind of attractor including chaos in the phase space of **u** spanned by all the Fourier modes, except for the phase factors of the modes. Power spectrum as well as Lyapunov exponent spectrum in a few-dimensional space embedded from a scalar time-series data have caught people's attention, but none of them has so much information on the total system of a time-dependent field as EFS. EFS is useful particularly for the system with many degrees of freedom. Figures 2(a), 4(a) and 5(a) are typical examples showing the access of the system to a point attractor. The periodic motion in Fig. 5(b) obviously shows the access to a limit cycle in the phase space. Figure 5(c) is similar, but it includes higher harmonics for $n_z = 3$. If more than two modes are periodic with different periods out of phase, the attractor is quasi-periodic. If many modes make almost-periodic irregular motions like in (the earlier part of) Fig. 6(a) and in (the whole) Fig. 8(a), the attractor is strange and the system is chaotic. Stabler looking high-energy modes in EFS express a large structure in the flow. It is possible to make a Poincaret map from EFS, but it is out of the scope of the present work to get into the details of chaos.

However, such a 2D unsteady state as we have seen hardly appears in reality because a 3D unsteady state arising due to the longitudinal modes ($k_x \neq 0$) of initial disturbances precedes far earlier, as is shown next.

4.2.2. *3D unsteady states.* In fact, with our antisymmetric boundary condition ($\Theta_w(z) = -z$) and for $Gr \sim 10^5$, the longitudinal modes of **u**, only if any of them are initially disturbed, begin to be excited to make the flow three-dimensional in an unsteady way. It is noteworthy here that we could hardly find a purely periodic (as is seen in 2D unsteady states) but an almost-periodic state based on interaction with longitudinal wave modes, even though our data was not exhaustive for all Gr. Figure 6(a) shows the evolution of $|\mathbf{u}(k_x, k_y, k_z)|^2$ for $L_x = 4\pi$ rather than $L_x = 3\pi$. We may judge from this that an initial transient motion ends at $t \fallingdotseq 5$ and an almost stationary unsteady motion ensues until $t \fallingdotseq 80$. After $t = 80$, the longitudinal modes indicated by lines with no marks (indicating $n_x = 1$ or 2) begin to weaken, so that a two-dimensional, two-convection-roll structure tends to predominate. For L_x much larger than 4π, however, a similar stationary unsteady motion continues much longer. (The unsteady motion continued until $t = 250$ for $L_x = 6\pi$.) Therefore, the case of $Gr = 480\,000$ is almost marginal between stable and unstable, so far as it is treated within the Boussinesq approximation.

Thus, the unsteady flow realized in Fig. 6(a) during $t = 5$–80 seems to be a prototype of an unsteady state, which would continue to occur if L_x is longer. During this time all modes are almost-periodic irregular, and then the system is in chaos with many degrees of freedom. Each wave mode is a Fourier-synthesis of multi-chromatic oscillations, and then various complicated travelling waves must sweep in all directions, in a more complicated way than Evans and Greif [7] described. However, the predominant wave modes have $n_x = 1$; that means, they have a strong possibility to sweep in the longitudinal direction. Figure 6(b) and (c) show the time-averaged (in $t = 20$–80) secondary flow and temperature contour of $\Theta + 1/2$ in a typical cross-section of the duct, respectively. In Fig. 6(c) are shown the experimental values by Mori and Koizumi [8] at various positions marked by symbols in the cross-section for comparison. A spanwise uniformity of time-averaged temperature is seen to be pretty much achieved also in this numerical simulation. Figures 7(a) and (b) show the instantaneous secondary flows and temperature contours in four typical equidistant cross-sections at $t = 60$. The time-averaged (in $t = 20$–40) Sherwood number contour for this case, but with $L_x = 3\pi$ for convenience, is seen in Fig. 3(b). Although the unsteady feature of flow is premature because of a shorter L_x, the tendency of flattening the deposition growth spanwise can be seen. Sh ranges from 4.77 to 20.09 in this case.

In Fig. 8(a) we can see the counterpart of Fig. 6(a) for $Gr = 4.8 \times 10^6$ and $L_x = 3\pi$. Obviously, the unsteady state lasts indefinitely, so that the system is more perfectly in chaos with many degrees of freedom than in Fig. 6(a). The time-averaged (in $t = 50$–200) secondary flow and temperature contour are seen in Figs. 8(b) and (c), respectively. The flow is more complex and the temperature boundary layers near the top and bottom wall are thinner than for $Gr = 480\,000$. The time-averaged (in $t = 20$–100) Sherwood number contour for this case is seen in Fig. 3(c), where the positive effect of a chaotic flow is clearly recognized. Sh ranges over 4.88–22.91. Here it is to be noted again that the pictures are much compressed in the longitudinal direction.

4.2.3. *Transition in Nusselt number.* In Fig. 9 is shown the time change of the Nusselt number averaged over the whole bottom surface for various Gr at $Re = 220$, only when $L_x = 3\pi$ is fixed. This clarifies the degree of chaotic feature changing with Gr reasonably well in one sense, such as to be expected if L_x is so finitely fixed. In this figure, the discussed chaotic nature of the flow with $Gr = 480\,000$ is only limited in the initial short period, and rather its stable character is dominantly seen. In fact, we should know that such a critical stability depends strongly on the longitudinal spatial period L_x, as described above, and the short period is effective for suppressing instability near the critical Gr. This means that the wavenumbers of predominant longitudinal unstable modes in these dynamics must be considerably low, at least within the

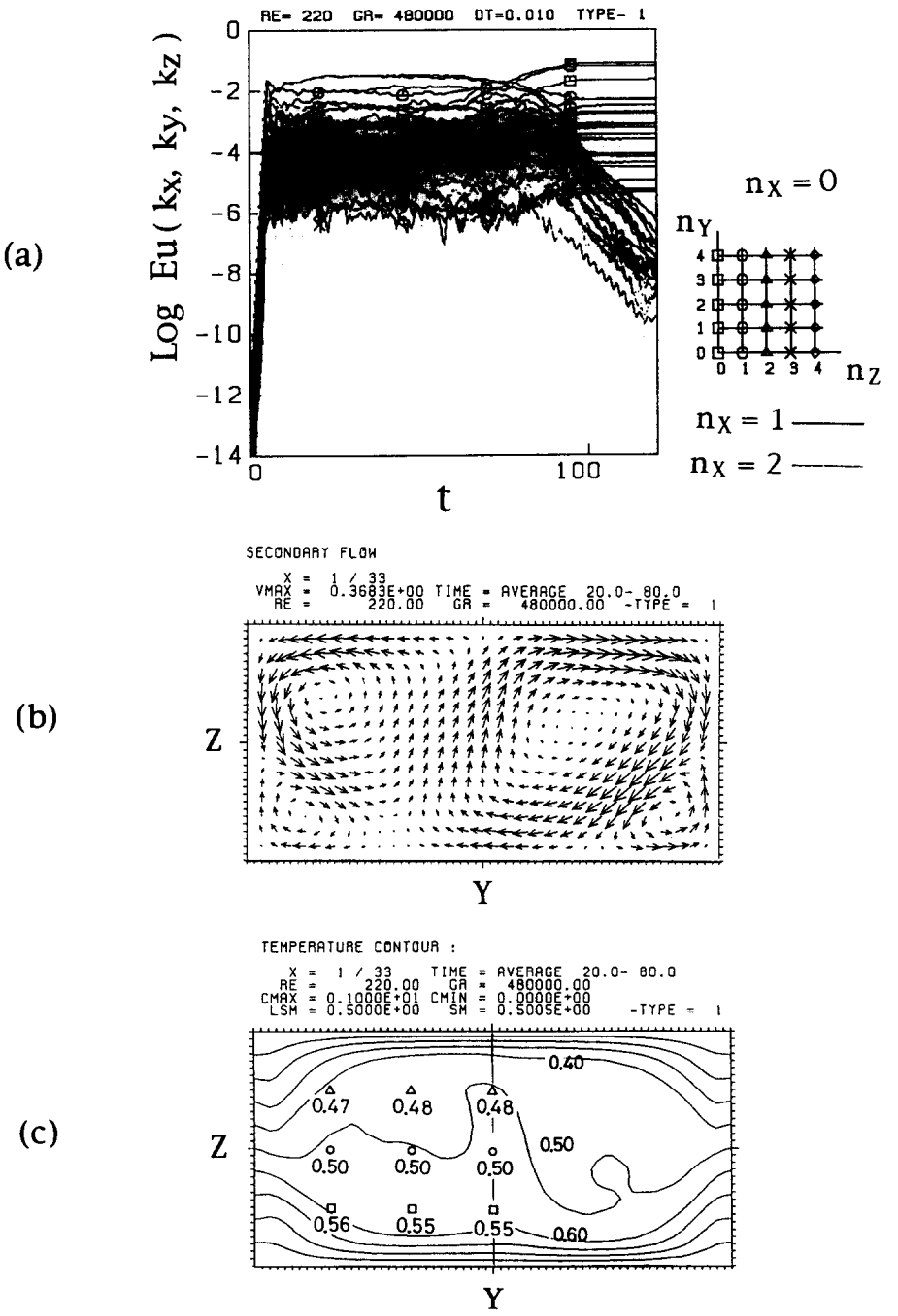

FIG. 6. (a) Evolution of $|\mathbf{u}(k_x, k_y, k_z)|^2$ for the case of $\Theta_w(z) = -z$, $Re = 220$, $Gr = 480\,000$ and $L_x = 4\pi$. (b) Time-averaged secondary flow in a typical cross-section for the same case. The magnitude of an arrow is normalized by the maximum secondary flow speed. (c) Time-averaged temperature contour for the same case. Experimental values by Mori and Koizumi [8] are added at various positions.

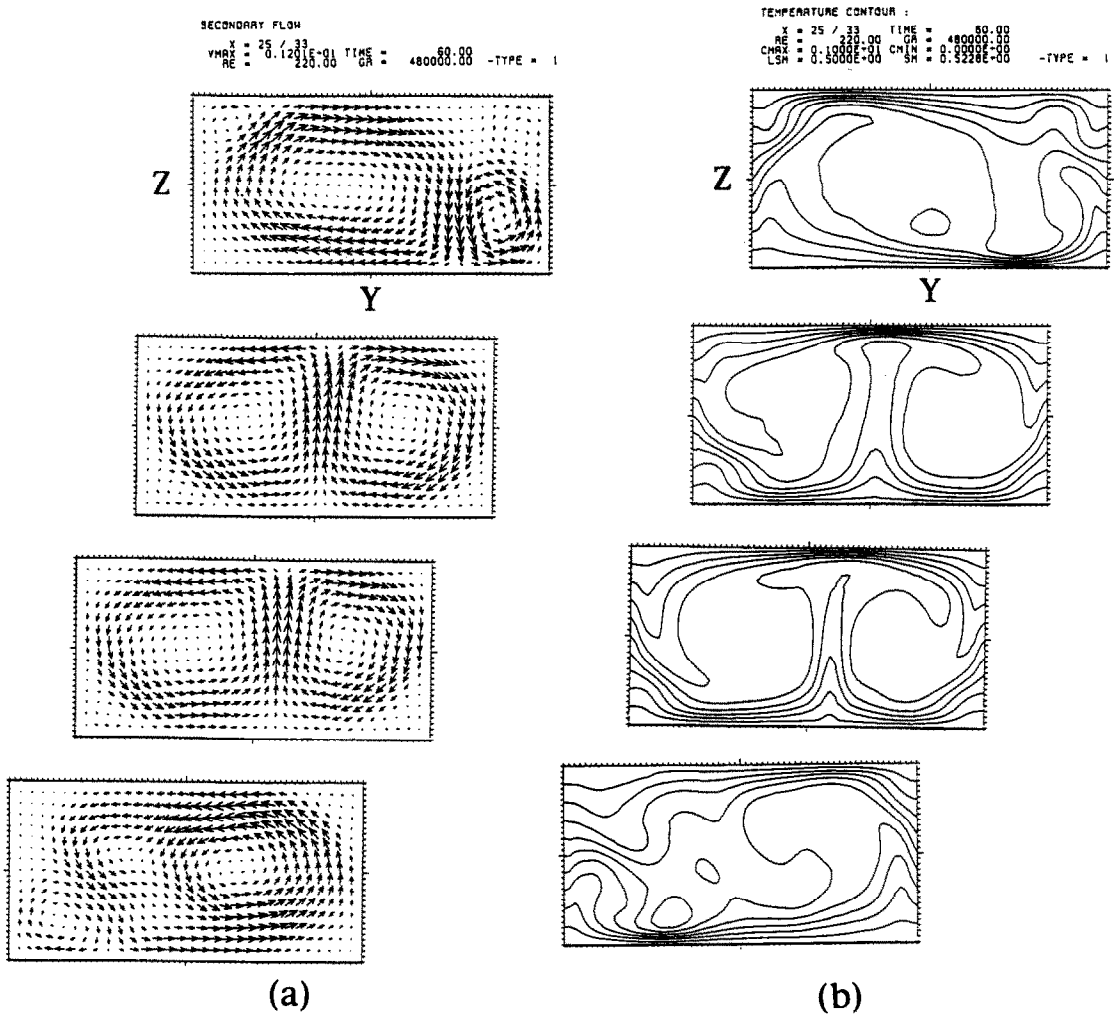

FIG. 7. (a) Instantaneous secondary flows in four typical equidistant ($x = 0$, $L_x/4$, $L_x/2$, $3L_x/4$) cross-sections at $t = 60$ for the case presented in Fig. 6. (b) Instantaneous temperature contours in the same cross-sections for the same case.

Boussinesq approximation. Therefore, if L_x is sufficiently large, the stable or quasi-stable part of the Nu curve in Figs. 9(a) or (b) might disappear and continue to be chaotic to different degrees, although this fact is hardly clarified by the present capacity of the computer.

4.2.4. *Comparison with experiment.* The unsteady flow experimentally found by Mori and Koizumi [8] for $Re = 220$ and $Gr = 480\,000$ seems to be, at least, qualitatively simulated by the present calculation, except that the experimental flow is never marginal but more chaotic. The consideration of the Lyapunov exponent spectrum in the three-dimensional space composed of time-delay coordinates from the experimentally observed temperature variation at a certain point in the duct was previously given [9, 10]. A similar calculation for the corresponding flow based on the present Boussinesq approach indicates also the spectrum of $(+, +, -)$, although the absolute values of the Lyapunov exponents do not coincide in both cases (they are much greater in experiment). In order to get a more realistic simulation, we would need to treat a real gas beyond the Boussinesq approximation. Both the feature of flow instability and the structure of chaos are considered to be more or less changed by this treatment, since a chaos depends on a specific nonlinear structure of system dynamics. In fact, the critical value of Gr indicating the beginning of the 3D unsteadiness is considered to be lower in real flows than the simulated ones by the Boussinesq approximation, judging from the comparison with experiment. A similar effect of departures from the Boussinesq approximation was recently assured in the Rayleigh–Bénard problem by Fröhlich *et al.* [20]. Of course, the antisymmetric solution described in 4.1 will be lost outside the Boussinesq approximation.

(a)

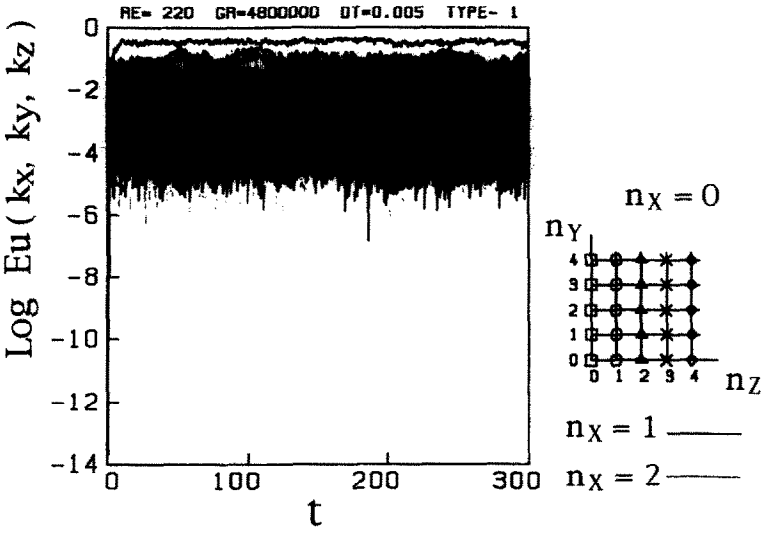

(b)

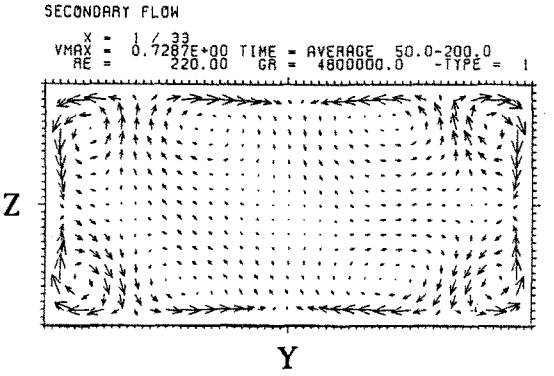

(c)

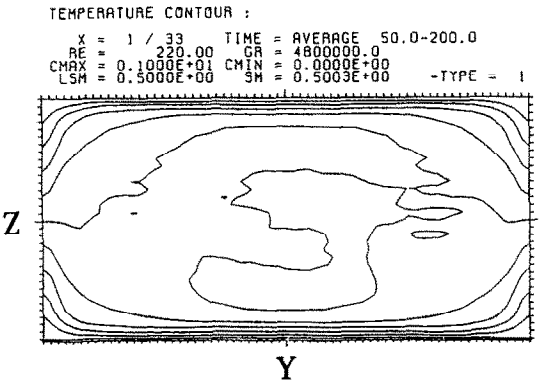

FIG. 8. (a) Evolution of $|\mathbf{u}(k_x, k_y, k_z)|^2$ for the case of $\Theta_w(z) = -z$, $Re = 220$, $Gr = 4.8 \times 10^6$ and $L_x = 3\pi$. (b), (c) The same as in Fig. 6.

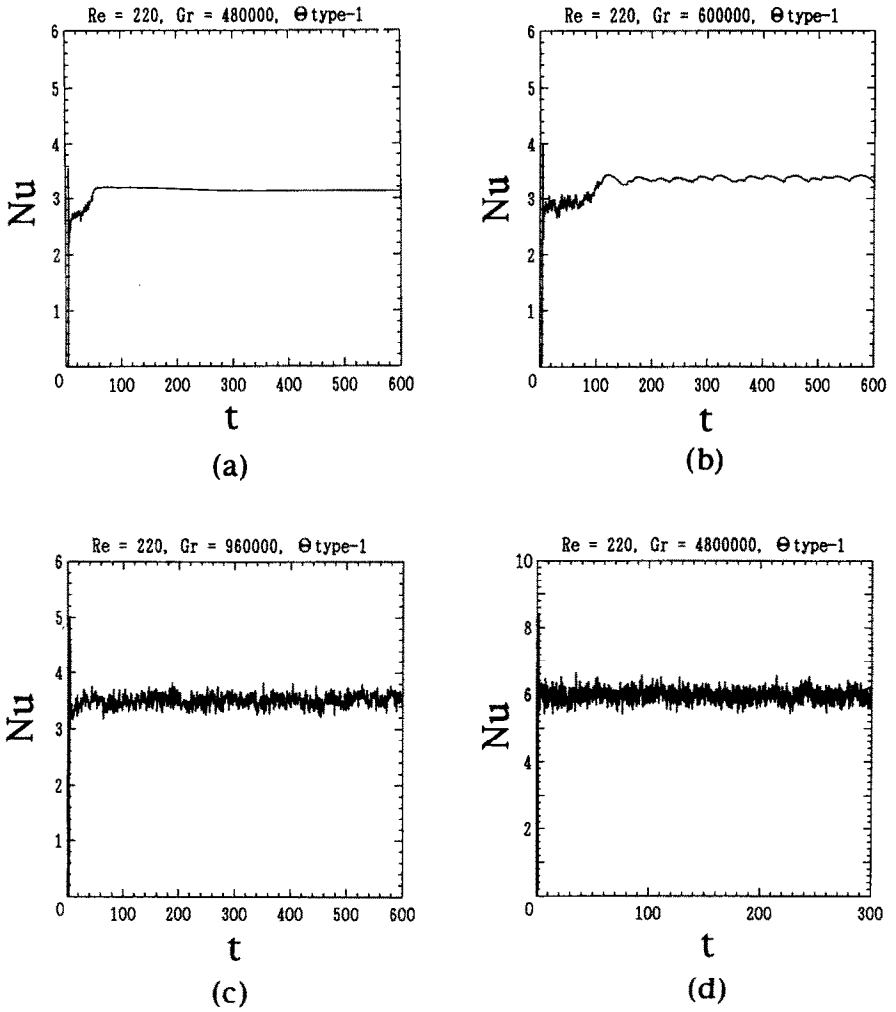

FIG. 9. Evolution of the Nusselt numbers averaged over the bottom for the case of $\Theta_w(z) = -z$, $Re = 220$, and $L_x = 3\pi$ for (a) $Gr = 480\,000$, (b) $Gr = 600\,000$, (c) $Gr = 960\,000$, and (d) $Gr = 4.8 \times 10^6$.

5. SUMMARY

Such a time-dependent problem as CVD flows in a rectangular duct can be well treated by a present-day supercomputer. A general trend of fully developed flows in a horizontal CVD duct has been clarified within the Boussinesq approximation, and the three-dimensionality and chaotic feature of unsteady flows which appear for some range of *Re* and *Gr* for aspect ratio 2 of the duct and on a proper side wall temperature condition have been studied. These flows were found to have the effect of flattening the deposition growth spanwise, as really evidenced also by experiment, and then seem to be useful for CVD manufactures and others. The slight longitudinal negative gradient of the growth may remain to be another problem in CVD, but it may be practically solved by adding a slight longitudinal temperature gradient on the substrate so as to accelerate the chemical reaction of deposition, or slightly tilting the substrate downstream so as to accelerate the flow and then to increase the flux of reactants.

Acknowledgement—The authors are grateful to Dr Y. Mori, Professor Emeritus of Tokyo Institute of Technology, for his valuable advice and continual encouragement, and are indebted to Dr T. Miyazaki and Dr H. Koizumi of the University of Electro-Communications for many discussions throughout this work.

REFERENCES

1. R. Takahashi, Y. Koga and K. Sugawara, Gas flow pattern and mass transfer analysis in a horizontal flow reactor for chemical vapor deposition, *J. Electrochem. Soc.* **119**, 1406–1412 (1972).
2. F. P. Incropera and J. A. Schutt, Numerical simulation of laminar mixed convection in the entrance region of

horizontal rectangular ducts, *Numer. Heat Transfer* **8,** 707–729 (1985).
3. H. V. Mahoney, F. P. Incropera and S. Ramadhyani, Development of laminar mixed convection flow in a horizontal rectangular duct with uniform bottom heating, *Numer. Heat Transfer* **12,** 137–155 (1987).
4. H. K. Moffat and K. F. Jensen, Complex flow phenomena in MOCVD reactors, *J. Crystal Growth* **77,** 108–119 (1986).
5. H. K. Moffat and K. F. Jensen, Three-dimensional flow effects in silicon CVD in horizontal reactors, *J. Electrochem. Soc.* **135,** 459–471 (1988).
6. T. A. Nyce, J. Quazzani, A. Durand-Daubin and F. Rosenberger, Mixed convection in a horizontal rectangular channel—experimental and numerical velocity distributions, *Int. J. Heat Mass Transfer* **35,** 1481–1494 (1992).
7. G. Evans and R. Greif, Unsteady three-dimensional mixed convection in a heated horizontal channel with applications to chemical vapor deposition, *Int. J. Heat Mass Transfer* **34,** 2039–2051 (1991).
8. Y. Mori and H. Koizumi, A study of controlling generation of a Benard cell in the laminar combined convection in a horizontal rectangular duct heated from below, *JSME Trans. B* **55,** 820–827 (1989); Y. Mori, Some optimizing examples in forced convective heat transfer, *ASME J. Heat Transfer* **112,** 268–273 (1990).
9. H. Koizumi and I. Hosokawa, Controlling the generation of Benard cells in combined convection in a horizontal rectangular duct heated from below (evidence of chaotic flows), *JSME Trans. B* **58,** 891–897 (1992).
10. Y. Mori, I. Hosokawa and H. Koizumi, Control of the formation of Benard cells in a horizontal rectangular duct heated from below, *Wärme- und Stoffübertragung* **27,** 195–200 (1992).
11. H. Koizumi and I. Hosokawa, Unsteady behavior and mass transfer performance of the combined convective flow in a horizontal rectangular duct heated from below, Submitted to *Int. J. Heat Mass Transfer.*
12. I. Hosokawa and K. Yamamoto, On direct numerical simulation of incompressible shear-flow turbulences by the Fourier-spectral method, *J. Phys. Soc. Japan* **55,** 1030–1031 (1986).
13. K. Yamamoto and I. Hosokawa, Numerical simulation of transition to turbulence in plane Poiseuille flow by a spectral method, *Nat. Aerospace Lab. Rep.* **SP-8,** 217–223 (1987).
14. I. Hosokawa, Numerical simulation of 3D and no-slip bounded flows in a horizontal chemical vapor deposition duct. In *Computers and Computing in Heat Transfer Science and Engineering* (Edited by W. Nakayama and K.-T. Yang), pp. 43–58. CRC Press, Boca Raton (1993).
15. S. Flügge, *Handbuch der Physik*, VIII/2, pp. 69–74. Springer, Berlin (1963).
16. C, Canuto, M. Y. Hussaini, A. Quarteroni and T. A. Zang, *Spectral Methods in Fluid Dynamics.* Springer, New York (1988).
17. N. Y. Lee, W. W. Schlutz and J. P. Boyd, Stability of fluid in a rectangular enclosure by spectral method, *Int. J. Heat Mass Transfer* **32,** 513–520 (1989).
18. K. Yamamoto, I. Hosokawa and H. Homma, Numerical simulation for controlling Benard cells in a rectangular duct by a spectral method, *Proc. 27th Nat. Heat transfer Symp. Japan, Nagoya,* **Vol. 3,** pp. 787–789 (1990).
19. K. Yamamoto, I. Hosokawa and Y. Tanaka, Numerical simulation of thermal convection in a rectangular duct flow, *Proc. 22th Turbulence Symp.—Nagare, Suppl.* Vol. 9, pp. 18–23 (1990).
20. J. Frölich, P. Laure and R. Peyret, Large departures from Boussinesq approximation in the Rayleigh–Bénard problem, *Phys. Fluids A* **4,** 1355–1371 (1992).